Optimizing Cement Distribution in the Fractured Area for Osteoporotic Vertebral Compression Fractures Through Biomechanical Effects Analysis Based on a Three Dimentional Lumbar Finite Element Modeling

Lin-qiang Ye
Guangzhou University of Traditional Chinese Medicine First Affiliated Hospital
De Liang
Guangzhou University of Traditional Chinese Medicine First Affiliated Hospital
Zhen Li
Dongguan Hospital of Traditional Chinese Medicine
Rui Weng
Guangzhou University of Chinese Medicine
Xue-cheng Huang
Southern Medical University
Yong-hong Feng
Dongguan Hospital of Traditional Chinese Medicine
Jian Zou
Dongguan Hospital of Traditional Chinese Medicine
Xiao-bing Jiang
Guangzhou University of Traditional Chinese Medicine First Affiliated Hospital
Guo-liang Lu (dglugl@163.com)
Department of Spinal Surgery, Dongguan Hospital of Traditional Chinese Medicine, Dongguan, Guangdong, People's Republic of China;

Research article

Keywords: Osteoporotic vertebral compression fracture, Percutaneous vertebral augmentation, Cement distribution, Finite element analysis, Fractured area

Posted Date: November 4th, 2020

DOI: https://doi.org/10.21203/rs.3.rs-100325/v1

Abstract

Background: While cement distributes sufficiently in the fractured area and relatively symmetrically around the fractured area, three types of cement mass location in the vertebral body are commonly seen when performing bipedicular percutaneous vertebral augmentation (PVA) for osteoporotic vertebral compression fractures (OVCFs), including anterolateral (AL), anteromedial (AM) and posterolateral (PL). However, little is known about differences of biomechanical behaviors among these three types of cement distribution so far. The present study aimed to investigate biomechanical effects of AL, AM and PL in the fractured area on OVCFs.

Methods: Three dimentional finite element methods were utilized to construct OVCF model and simulate AL, AM and PL in the fractured area for OVCFs treated with PVA. Distributions and magnitudes of von Mises stress in cortical and cancellous bone and maximum displacement of the four models were compared.

Results: Compared with the OVCF model, Distribution of von Mises stress in cortical bone was unchanged while that in cancellous bone was transferred to be concentrated symmetrically at cancellous bone surrounding cement after PVA. Maximum displacement and maximum von Mises stress in cortical bone in AL decreased the most significantly, while AM created the lowest maximum von Mises stress in cancellous bone.

Conclusions: Cement distribution between AL and AM may balance stress in cortical and cancellous bone, better restoring vertebral strength, meanwhile, providing sufficient vertebral stability.

Introduction

Osteoporotic vertebral compression fractures (OVCFs) are very common in the elderly, with an estimated 1.4 million new fractures occurring every year worldwide [1]. Until recently, symptomatic OVCFs were treated commonly with conservative methods including bed rest, analgesics, braces, and physical therapy. However, percutaneous vertebral augmentation (PVA), such as percutaneous vertebraplasty and percutaneous kyphoplasty, has been introduced as an alternative treatment option [2, 3]. Biomechanical studies showed significant increases in the stiffness and strength of individual fractured vertebra after PVA [4, 5]. Apart from rapid pain relief, another immediate effect of PVA was an increase of anterior vertebral height, which reduced kyphosis in patients [6–8]. The realigned spinal column and regained height in the augmented vertebra may decrease pulmonary and gastro-intestinal complications and early morbidity related to compression fractures [9].

Our previous biomechanical study demonstrated that various cement distributions relative to the fractured area could produce different impacts on biomechanical behaviors of OVCFs treated with PVA [10]. Biomechanical behaviors of sufficient versus insufficient cement distributions in the fractured area and symmetrical versus asymmetrical cement distributions around the fractured area were compared. Insufficient cement distribution in the fractured area led to significant increase in maximum displacement

of augmented vertebra, which might explain unrelieved pain after PVA in treatment of symptomatic OVCFs. While insufficient cement distribution in the fractured area increased maximum von Mises stress in cortical and cancellous bone of augmented vertebra significantly, asymmetrical cement distribution around the fractured area increased maximum von Mises stress in cancellous bone significantly, both of which might be the reason for recollapse of augmented vertebra. These findings were verified by related clinical studies [11, 12].

While cement distributes sufficiently in the fractured area and relatively symmetrically around the fractured area, three types of cement mass location in the vertebral body are commonly seen according to our clinical practice when performing bipedicular PVA for OVCFs, including anterolateral (AL), anteromedial (AM) and posterolateral (PL). To the best of our knowledge, however, few biomechanical studies exist that show the differences of biomechanical behaviors among these three types of cement distribution so far. In order to further optimize cement distribution in the fractured area for OVCFs treated with PVA, this study was performed to investigate biomechanical effects of AL, AM and PL in the fractured area on OVCF on the basis of our previous study [10].

Methods

Development of normal L1-L5 finite element (FE) model

A normal three-dimensional digital anatomical FE model of L1-L5 was created based on CT images of a L1-L5 motion segment without injury or radiographic evidence of degeneration. The image data were from a 26-year-old male who requested CT scan for health examination at our hospital. He was explained about the research purpose and signed the consent form. Slice thickness was 0.625 mm. The slice images were preserved in a computer and then imported to Mimics 19.0 software (Materialise Inc., Leuven, Belgium) for generation of the 3-dimensional geometries of L1-L5 vertebra. Then, a smoothing process was performed in Geomagic Studio 2013 software (Geomagic Inc., Research Triangle Park, NC, USA) to remove spikes and holes on the surface of the vertebral geometries. The geometries of intervertebral discs which were difficult to separate from the CT images, were created using SolidWorks 2017 sofeware (SolidWorks Inp., Concord, MA, USA). Each vertebra consisted of a cancellous core surrounded by a cortical shell layer with thickness of 0.5 mm [13]. Cartilaginous endplates were simulated with thickness of 0.5 mm at both ends of each vertebra [14]. The nucleus pulpous occupied about 43% of the total disc [15]. Facet joints were modeled with a cartilage layer with thickness of 0.2 mm and a gap of about 0.6 mm [16]. Element types of cancellous bone, posterior bony element, cartilaginous endplates, annulus and nucleus pulpous were defined as solid elements. Cortical bone and facet joint cartilage were defined as shell elements. In order to mimic collagen fibers of annulus fibrosus, four layers of collagen fibers were embeded radially in the annular ground substances. For each layer two bundles of fibers were modeled with orientation of about ± 30 ° with respect to the horizontal plane using truss elements [17]. A fiber cross-sectional area of 0.1mm^2 was assumed [18]. Ligaments were modeled with truss elements. The assigned material properties were assumed to be homogeneous, linear, and

isotropic and truss elements were tension-only. Tied constraints were used to ensure disc and ligament attachments to the vertebra and prevent any relative movement during the simulations. Frictionless Surface-based, finite sliding contact was defined for facet joint cartilages [19]. Material properties were taken from the literatures and listed in Table 1 [18, 20, 21]. Abaqus 6.12 (Abaqus, Inc., Providence, RI, USA) was used for numerical analysis. A mesh convergence study was conducted and considered to be convergent when the prediction results obtained by two consecutive mesh resolutions had differences smaller than 5% [22, 23]. The final mesh consisted of 8042 solid elements, 177037 shell elements, 3840 truss elements and a total of 285469 nodes (Fig. 1).

Table 1
Material properties of different structures in the finite element models

Component name	Young's modulus (MPa)	Poisson's ratio	Cross-section area (mm^2)
Cortical bone	12000 (osteoporotic: 8040)	0.3	/
Cancellous bone	100 (osteoporotic: 34)	0.2	/
Posterior structure	3500 (osteoporotic: 2345)	0.25	/
Cartilaginous endplate	23.8 (osteoporotic: 15.9)	0.4	/
Nucleus pulposus	1	0.495	/
Annulus: ground substance	4.2	0.45	/
Annulus: fiber	25	0.3	0.1
Facet joint Cartilage	23.8	0.4	-
ALL	20	0.3	40
PLL	70	0.3	20
LF	50	0.3	40
CL	50	0.3	30
ISL	20	0.3	40
SSL	28	0.3	30
ITL	28	0.3	10
Cement	3000	0.4	/

All = anterior longitudinal ligament; PLL = posterior longitudinal ligament; LF = ligamantum flavum; CL = capsular ligament; ISL = interspinous ligament; SSL = supraspinal ligament; ITL = intertransverse ligament.

Model Validation Method

To validate the normal FE model, rang of motion (ROM) and intradiscal pressure (IDP) were the parameters chosen for validation. For ROM, the inferior endplate of L5 vertebra was fixed in all degrees of freedom and Loads were applied in L1 superior endplate. Pure moment of 7.5 N m in flexion/extension,

left/right lateral bending, and left/right axial rotation were independently applied. The ROMs in each spinal level were recorded. For IDP, pure compressive forces of 300N and 1000N were independently applied between the L4 and L5 levels, the IDPs in L4-L5 disc were recorded. The simulation results predicted by the FE model were compared with corresponding experimental data reported in the literatures [24, 25].

Development Of Osteoporotic L1-l5 Fe Model

Because OVCF is investigated, model of an osteoporotic L1-L5 was built. According to methods reported by Polikeit et al [21], a model with osteoporosis was defined as follows. The elastic moduli of all bony structures were reduced, by 66% for the cancellous bone, and by 33% for the cortical shell, the endplates, and the posterior elements. The other structures were left unchanged. Material properties were listed in Table 1.

Simulation Of Ovcf

Referring to simulation method reported by Chiang et al. [26], the model (Pre-augmented) was constructed with the following steps to simulate OVCF on L3. A cleft was horizontally penetrated into the vertebral body by 20 mm through the center of the anterior cortical shell. The size of the cleft was approximately 20 mm, 30 mm and 2 mm in depth, width and height, respectively (Fig. 2).

Simulation Of Cement Augmentation

For bone cement material, PMMA was applied because it represents the most common clinically used material. Its material property was listed in Table 1 [21]. Two cement cylinders with the same volume were vertically implanted around the fractured area symmetrically to mimic bipedicular PVA with sufficient cement distribution in the fractured area and symmetrical cement distribution around the fractured area. The volume of each cement cylinder was approximately 3 ml. For simulation of AL, both of cement cylinders were embedded in the anterior column and in proximity to the lateral border of the vertebral body. Subsequently, the two cement cylinders were relocated medially adjacent to midline of the vertebral body to mimic AM. Being different from AM, the two cement cylinders of AL were relocated posteriorly with partial cement cylinders locating in middle column to simulate PL. Eventually, we got four different models for test, including the fractured model before PVA and three augmented models (Fig. 2).

Loads And Boundary Conditions

A pure moment of 7.5 N m was applied independently for flexion/extension, left/right lateral bending, and left/right axial rotation. The inferior endplate of L5 vertebra was fixed in all degrees of freedom and Loads were applied in L1 superior endplate. Abaqus 6.12 (Abaqus, Inc., Providence, RI, USA) was used for

numerical analysis. The magnitudes and distributions of von Mises stress in cortical and cancellous bone and maximum displacement of L3 vertebral body were recorded. Von Mises stress has been proposed as a parameter of failure criteria for bone [21, 27] and maximum displacement a parameter of stability [28].

Results

Validation of the normal L1-L5 FE model

Under 7.5 N m pure moments, the ROMs of flexion, extension, lateral bendings and axial rotations in each spinal level predicted by the FE model were within the ranges reported by Panjiabi et al. (Fig. 3a-d)[24]. L4-L5 IDPs under compressive forces of 300N and 1000N were in agreement with the results of the in vitro study (Fig. 3e) [25].

Distributions and magnitudes of von Mises stress in cortical bone of L3 in OVCF models before and after PVA

The results of distributions of von Mises stress under flexion in cortical bone of L3 in OVCF models before and after PVA were shown in Fig. 4a. Compared with distribution before PVA, it was unchanged after PVA, which was still concentrated at posterior unfractured area. Similar results could be seen in extension, lateral bendings and axial rotations.

Regarding magnitude of maximum von Mises stress in cortical bone of L3, it decreased significantly after PVA under all loading conditions with that in AL decreasing the most significantly. Comparing AM with PL, it was lower in AM under flexion, extension and axial rotations while it was lower in PL under lateral bendings (Fig. 5a).

Distributions and magnitudes of von Mises stress in cancellous bone of L3 in OVCF models before and after PVA

The results of distributions of von Mises stress under flexion in cancellous bone of L3 for OVCF models before and after PVA were shown in Fig. 4b, and demonstrated that von Mises stress was concentrated at posterior unfractured area before PVA, but transferred to be concentrated at cancellous bone surrounding bone cement after PVA. However, differences were not detected among augmented models, in which von Mises stress was concentrated below and above fractured area symmetrically. Similar results could be seen in extension, lateral bendings and axial rotations.

Regarding magnitude of maximum von Mises stress in the cancellous bone of L3, it increased after PVA under flexion and lateral bendings while decreased under extension (with exception of PL) and axial rotations. It was lowest in AM under all the loading conditions among AL, AM and PL. Comparing AL with PL, it was lower in AL under flexion and extension while it was lower in PL under lateral bendings, the differences under axial rotations were not obvious (Fig. 5b).

Maximum displacement of L3 for OVCF models before and after PVA

Regarding maximum displacement of L3, it decreased significantly after PVA under all loading conditions with that in AL decreasing the most significantly. Comparing AM with PL, it was lower in AM under flexion, extension and axial rotations while it was lower in PL under lateral bendings (Fig. 5c).

Discussion

This finite element model was developed on the data collected from a spinal CT scan of a healthy lumbar spine and biomechanical material properties reflecting the pathological characteristics of vertebral osteoporosis. A validated five-vertebra segment was constructed, but not individual vertebra, because a five-vertebra segment model with intervertebral discs and facet joints might not only highly simulated the motion and load transfer of lumbar spine when OVCF was simulated in the middle vertebra, but also avoid loading positions and boundary conditions being directly connected to the target vertebra of L3, which may have an influence on biomechanical behaviors of L3 [29]. The validation test proved that the constructed three-dimensional finite element model could accurately simulate physiological activity and load transfer at the lumbar spine and, therefore, could be a valuable tool for later research. Although stress measurements of cortical and cancellous bone were not validated experimentally, this could not be an influential factor in our study because the parameters in this study were compared in terms of relative differences among fractured models before and after PVA with different distributing patterns of cement.

The anterior cortex of compressed vertebra is usually injured and not continuous before union. In the current study, we attempted to re-create a compression fracture model where a cleft was horizontally penetrated into L3 vertebral body through the center of the anterior cortical shell. This failure model may be attributed to the type A1.2 fracture, that is, the wedge impaction fracture [30]. For bipedicular augmentation, two vertically orientated cement cylinders were implanted in the vertebral body. Similar methods to simulate PVA had been reported by Polikeit et al.[31] and Liebschner et al.[32], and they also agreed that this shape was comparable with the cement distribution seen on radiographs of treated patients. We acknowledge that using cylinders to simulate PVA is done for ease of computer simulation, and not a direct reflection of the reality of PVA. Because the simulation of PVA in the current study can be easily created through finite element analysis method and ensure the repeatability of the study. We are aware that different shapes of cement might occur in the vertebral bodies. Thus, preliminary experiments, in which another shape of cement (cement cake) with equivalent volume was used to simulate PVA, had been done to analyze how cement shape affect findings in our previous study. We found that different stress and displacement can be produced using cement cakes to simulate PVA, but the same conclusion can be drawn using cement cakes to simulate PVA like cement cylinders. In addition, because our previous study demonstrated that sufficient cement distribution in the fractured area and symmetrical cement distribution around the fractured area may provide better structural support, as compared with insufficient and asymmetrical cement distribution [10]. In this study, the two cement cylinders were implanted around the fractured area symmetrically to mimic bipedicular PVA with sufficient cement distribution in the fractured area and symmetrical cement distribution around the fractured area. Using

this simulation method may relatively accurately reflect different biomechanical effects of AL, AM and PL in the fractured area on OVCFs.

Our current study is focus on distributions and magnitudes of von Mises stress in cortical and cancellous bone and maximum displacement of L3 for OVCF models before and after PVA. Distribution of von Mises stress in cortical bone was unchanged while that in cancellous bone was transferred to be concentrated symmetrically at cancellous bone surrounding cement after PVA, which is consistent with our previous study [10] and a finite element analysis conducted by Polikeit et al. [21]. This is likely due to the fact that increase in vertebral stability of OVCF after PVA depends on interdigitation between cement and cancellous bone. In addition, it is known that back pain caused by OVCFs is mostly likely to be related to periosteal nerves aggravated by micromotion at the fractured area and recollapse is due to reduced strength of OVCFs. Thus, stabilization of the fractured area and restoration of vertebral strength are the most acceptable mechanisms for pain relief and preventing recollapse after PVA in treatment of OVCFs. Interestingly, we discovered that maximum displacement of L3 decreased significantly after PVA under all loading conditions with that in AL decreasing the most significantly. It indicates that vertebral stability can be better restored by AL. Furthermore, maximum von Mises stress in cortical bone of L3 had the same trend as maximum displacement of L3, which implys that AL can better restore vertebral strength in terms of stress in cortical bone. However, AM created the lowest maximum von Mises stress in cancellous bone of L3, which suggests that AM can better restore vertebral strength in terms of stress in cancellous bone. Given that both cortical and cancellous bone contribute to vertebral strength, we believe that cement distribution between AL and AM can balance stress in cortical and cancellous bone, better restoring vertebral strength. Meanwhile, since difference of maximum displacement of L3 between AL and AM was not obvious, sufficient vertebral stability can be provided with cement distribution between AL and AM.

Some limitations of this study need to be mentioned. Firstly, according to our previous study, location of fractured area of OVCFs could be classified into 3 types including superior, middle, and inferior [11]. Some OVCFs involve one part while others may involve two or three parts. The current model only focused on OVCFs with middle fractured area. Secondly, wedge-like vertebra simulating compression fracture was not created. Only the idealized status of anterior vertebral height correction was simulated in this study, however, PVA only partially restore the vertebral shape in most cases. Third, simulation of cement augmentation with cement cylinders is not a direct reflection of the reality of PVA. Above shortcomings may limit the application of the results to real world clinical scenarios. Clinical study evaluating the findings from this study would be expected in the future.

Conclusions

While cement distributes sufficiently in the fractured area and relatively symmetrically around the fractured area, various cement mass location in the vertebral body including AL, AM and PL have differences in restoring vertebral stability and strength of OVCFs due to the fact that different stress and displacement of corresponding augmented models were produced. Cement distribution between AL and

AM may balance stress in cortical and cancellous bone, better restoring vertebral strength, meanwhile, providing sufficient vertebral stability.

Abbreviations

OVCF
Osteoporotic vertebral compression fracture; PVA:Percutaneous vertebral augmentation; AL:Anterolateral; AM:Anteromedial; PL:Posterolateral; FE:Finite element; ROM:Rang of motion; IDP:Intradiscal pressure

Declarations

Acknowledgements

Not applicable

Authors' contributions

YLQ, JXB and LGL contributed to conceiving and designing the study. YLQ, WR and HXC performed the experiment. YLQ, LZ, FYH and ZJ analyzed the data. YLQ play the main role in writing the article. All authors read and approved the final manuscript.

Funding

The research was supported by Medical Science and Technology Foundation of Guangdong Province (NO.A2017024) and Traditional Chinese Medicine Bureau of Guangdong Province (NO.20182030).

Availability of data and materials

All data and materials are contained within the manuscript.

Ethics approval and consent to participate

This study was granted an exemption from requiring ethics approval by the ethics board of The First Affiliated Hospital of Guangzhou University of Chinese Medicine. Written consent was obtained from the participant.

Consent for publication

Not applicable.

Competing interests

The authors declare no conflict of interest.

References

1. Johnell O, Kanis JA. An estimate of the worldwide prevalence and disability associated with osteoporotic fractures. Osteoporos Int. 2006; 17:1726-33.
2. Lou S, Shi X, Zhang X, Lyu H, Li Z, Wang Y. Percutaneous vertebroplasty versus non-operative treatment for osteoporotic vertebral compression fractures: a meta-analysis of randomized controlled trials. Osteoporos Int. 2019; 30:2369-80.
3. Beall DP, Chambers MR, Thomas S, Amburgy J, Webb JR, Jr., Goodman BS, Datta DK, Easton RW, Linville D, 2nd, Talati S, Tillman JB. Prospective and Multicenter Evaluation of Outcomes for Quality of Life and Activities of Daily Living for Balloon Kyphoplasty in the Treatment of Vertebral Compression Fractures: The EVOLVE Trial. Neurosurgery. 2019; 84:169-78.
4. Belkoff SM, Mathis JM, Jasper LE, Deramond H. The biomechanics of vertebroplasty. The effect of cement volume on mechanical behavior. Spine (Phila Pa 1976). 2001; 26:1537-41.
5. Chen B, Li Y, Xie D, Yang X, Zheng Z. Comparison of unipedicular and bipedicular kyphoplasty on the stiffness and biomechanical balance of compression fractured vertebrae. Eur Spine J. 2011; 20:1272-80.
6. Teng MM, Wei CJ, Wei LC, Luo CB, Lirng JF, Chang FC, Liu CL, Chang CY. Kyphosis correction and height restoration effects of percutaneous vertebroplasty. AJNR Am J Neuroradiol. 2003; 24:1893-900.
7. McKiernan F, Faciszewski T, Jensen R. Reporting height restoration in vertebral compression fractures. Spine (Phila Pa 1976). 2003; 28:2517-21; disucssion 3.
8. Hiwatashi A, Moritani T, Numaguchi Y, Westesson PL. Increase in vertebral body height after vertebroplasty. AJNR Am J Neuroradiol. 2003; 24:185-9.
9. Garfin SR, Yuan HA, Reiley MA. New technologies in spine: kyphoplasty and vertebroplasty for the treatment of painful osteoporotic compression fractures. Spine (Phila Pa 1976). 2001; 26:1511-5.
10. Liang D, Ye LQ, Jiang XB, Yang P, Zhou GQ, Yao ZS, Zhang SC, Yang ZD. Biomechanical effects of cement distribution in the fractured area on osteoporotic vertebral compression fractures: a three-dimensional finite element analysis. J. Surg. Res. 2015; 195:246-56.
11. Ye LQ, Liang, Jiang XB, Yao ZS, Lu H, Qiu T, Yu WB, Mo L, Zhang SC, Jin DX. Risk Factors for the Occurrence of Insufficient Cement Distribution in the Fractured Area after Percutaneous Vertebroplasty in Osteoporotic Vertebral Compression Fractures. Pain Physician. 2018; 21:E33-E42.
12. Lin WC, Lee YC, Lee CH, Kuo YL, Cheng YF, Lui CC, Cheng TT. Refractures in cemented vertebrae after percutaneous vertebroplasty: a retrospective analysis. Eur Spine J. 2008; 17:592-9.
13. Wang Md K, Jiang Ph DC, Wang Ph DL, Wang Md H, Niu Ph DW. The biomechanical influence of anterior vertebral body osteophytes on the lumbar spine: A finite element study. Spine J. 2018; 18:2288-96.
14. Newell N, Little JP, Christou A, Adams MA, Adam CJ, Masouros SD. Biomechanics of the human intervertebral disc: A review of testing techniques and results. J Mech Behav Biomed Mater. 2017; 69:420-34.

15. Polikeit A, Ferguson SJ, Nolte LP, Orr TE. Factors influencing stresses in the lumbar spine after the insertion of intervertebral cages: finite element analysis. Eur Spine J. 2003; 12:413-20.
16. Schmidt H, Heuer F, Wilke HJ. Which axial and bending stiffnesses of posterior implants are required to design a flexible lumbar stabilization system? J Biomech. 2009; 42:48-54.
17. Ottardi C, Galbusera F, Luca A, Prosdocimo L, Sasso M, Brayda-Bruno M, Villa T. Finite element analysis of the lumbar destabilization following pedicle subtraction osteotomy. Med Eng Phys. 2016; 38:506-9.
18. Galbusera F, Bellini CM, Anasetti F, Ciavarro C, Lovi A, Brayda-Bruno M. Rigid and flexible spinal stabilization devices: a biomechanical comparison. Med Eng Phys. 2011; 33:490-6.
19. Dreischarf M, Zander T, Shirazi-Adl A, Puttlitz CM, Adam CJ, Chen CS, Goel VK, Kiapour A, Kim YH, Labus KM, Little JP, Park WM, Wang YH, Wilke HJ, Rohlmann A, Schmidt H. Comparison of eight published static finite element models of the intact lumbar spine: predictive power of models improves when combined together. J Biomech. 2014; 47:1757-66.
20. Cheung JT, Zhang M, Chow DH. Biomechanical responses of the intervertebral joints to static and vibrational loading: a finite element study. Clin Biomech (Bristol, Avon). 2003; 18:790-9.
21. Polikeit A, Nolte LP, Ferguson SJ. The effect of cement augmentation on the load transfer in an osteoporotic functional spinal unit: finite-element analysis. Spine (Phila Pa 1976). 2003; 28:991-6.
22. Jones AC, Wilcox RK. Finite element analysis of the spine: towards a framework of verification, validation and sensitivity analysis. Med Eng Phys. 2008; 30:1287-304.
23. Ayturk UM, Puttlitz CM. Parametric convergence sensitivity and validation of a finite element model of the human lumbar spine. Comput Methods Biomech Biomed Engin. 2011; 14:695-705.
24. Panjabi MM, Oxland TR, Yamamoto I, Crisco JJ. Mechanical behavior of the human lumbar and lumbosacral spine as shown by three-dimensional load-displacement curves. J Bone Joint Surg Am. 1994; 76:413-24.
25. Brinckmann P, Grootenboer H. Change of disc height, radial disc bulge, and intradiscal pressure from discectomy. An in vitro investigation on human lumbar discs. Spine (Phila Pa 1976). 1991; 16:641-6.
26. Chiang CK, Wang YH, Yang CY, Yang BD, Wang JL. Prophylactic vertebroplasty may reduce the risk of adjacent intact vertebra from fatigue injury: an ex vivo biomechanical study. Spine (Phila Pa 1976). 2009; 34:356-64.
27. Maknickas A, Alekna V, Ardatov O, Chabarova O, Zabulionis D, Tamulaitienė M, Kačianauskas R. FEM-Based Compression Fracture Risk Assessment in Osteoporotic Lumbar Vertebra L1. Appl. Sci 2019; 9, 3013.
28. Li QL, Li XZ, Liu Y, Zhang HS, Shang P, Chu ZM, Chen JC, Chen M, Qin R. Treatment of thoracolumbar fracture with pedicle screws at injury level: a biomechanical study based on three-dimensional finite element analysis. Eur J Orthop Surg Traumatol. 2013; 23:775-80.
29. Wijayathunga VN, Oakland RJ, Jones AC, Hall RM, Wilcox RK. Vertebroplasty: Patient and treatment variations studied through parametric computational models. Clin Biomech (Bristol, Avon). 2013; 28:860-5.

30. Magerl F, Aebi M, Gertzbein SD, Harms J, Nazarian S. A comprehensive classification of thoracic and lumbar injuries. Eur Spine J. 1994; 3:184-201.
31. Polikeit A, Nolte LP, Ferguson SJ. The effect of cement augmentation on the load transfer in an osteoporotic functional spinal unit: finite-element analysis. Spine (Phila Pa 1976). 2003; 28:991-6.
32. Liebschner MA, Rosenberg WS, Keaveny TM. Effects of bone cement volume and distribution on vertebral stiffness after vertebroplasty. Spine (Phila Pa 1976). 2001; 26:1547-54.

Figures

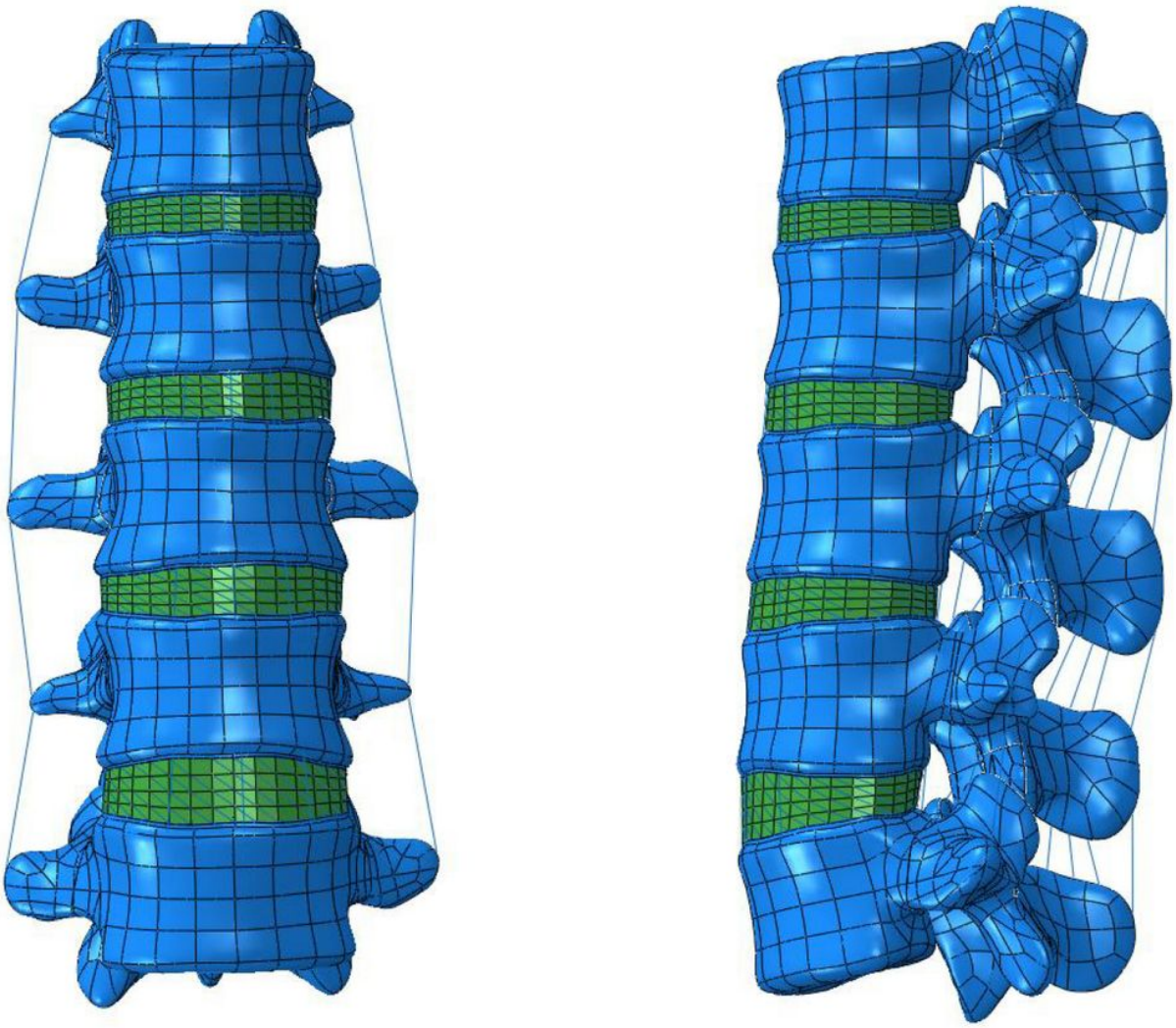

Figure 1

Normal L1-L5 FE model.

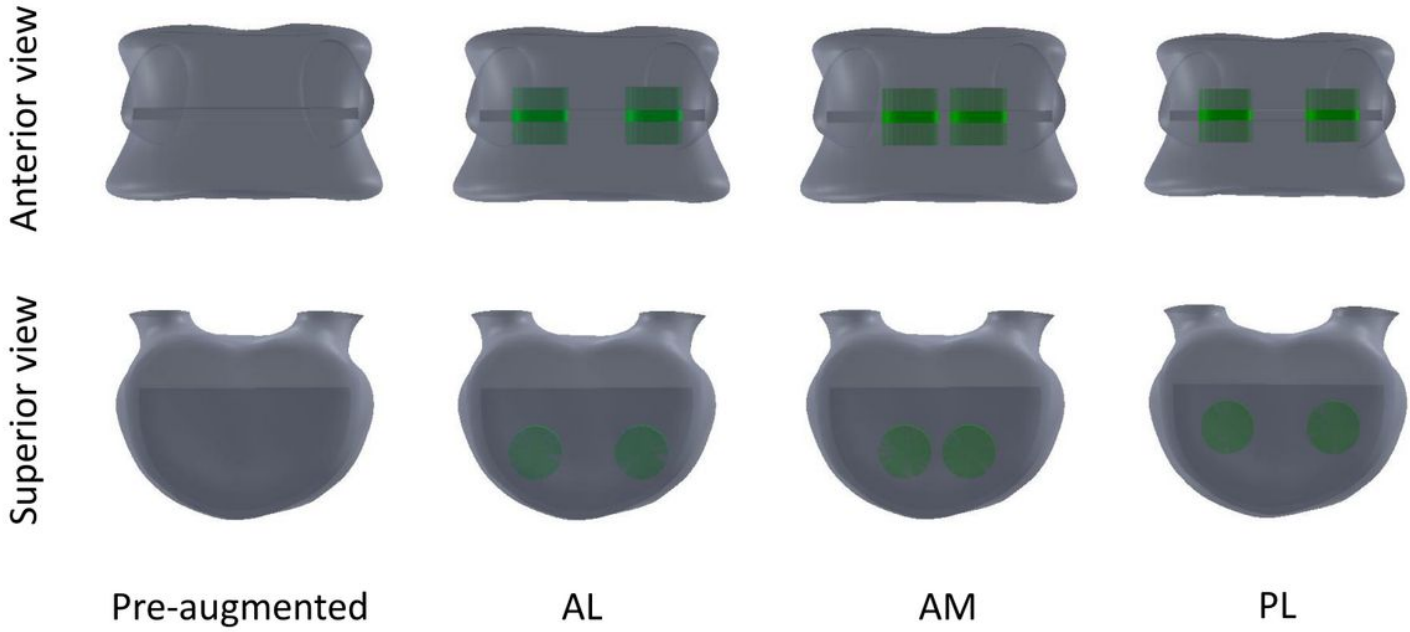

Figure 2

OVCF models before and after PVA.

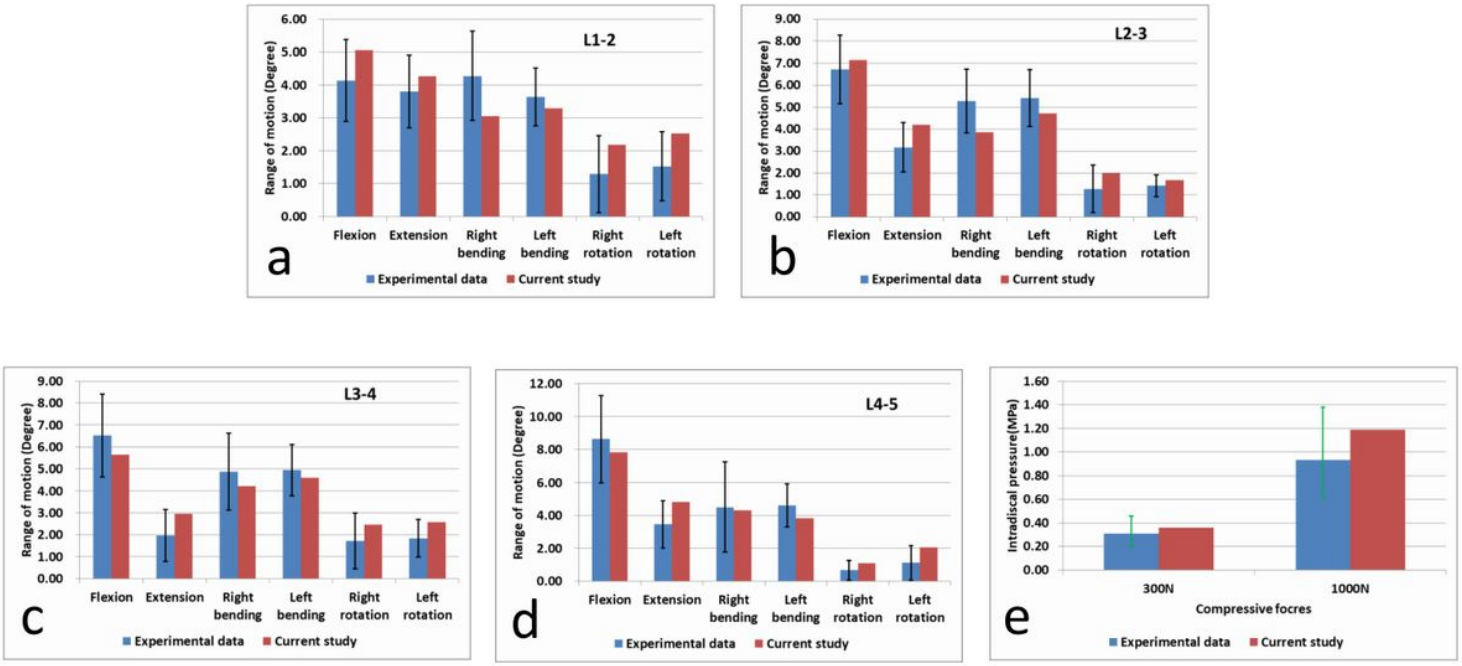

Figure 3

Normal L1-L5 FE model validation (The black bars refer to the standard deviations. The green bars show the in vitro range of results.)

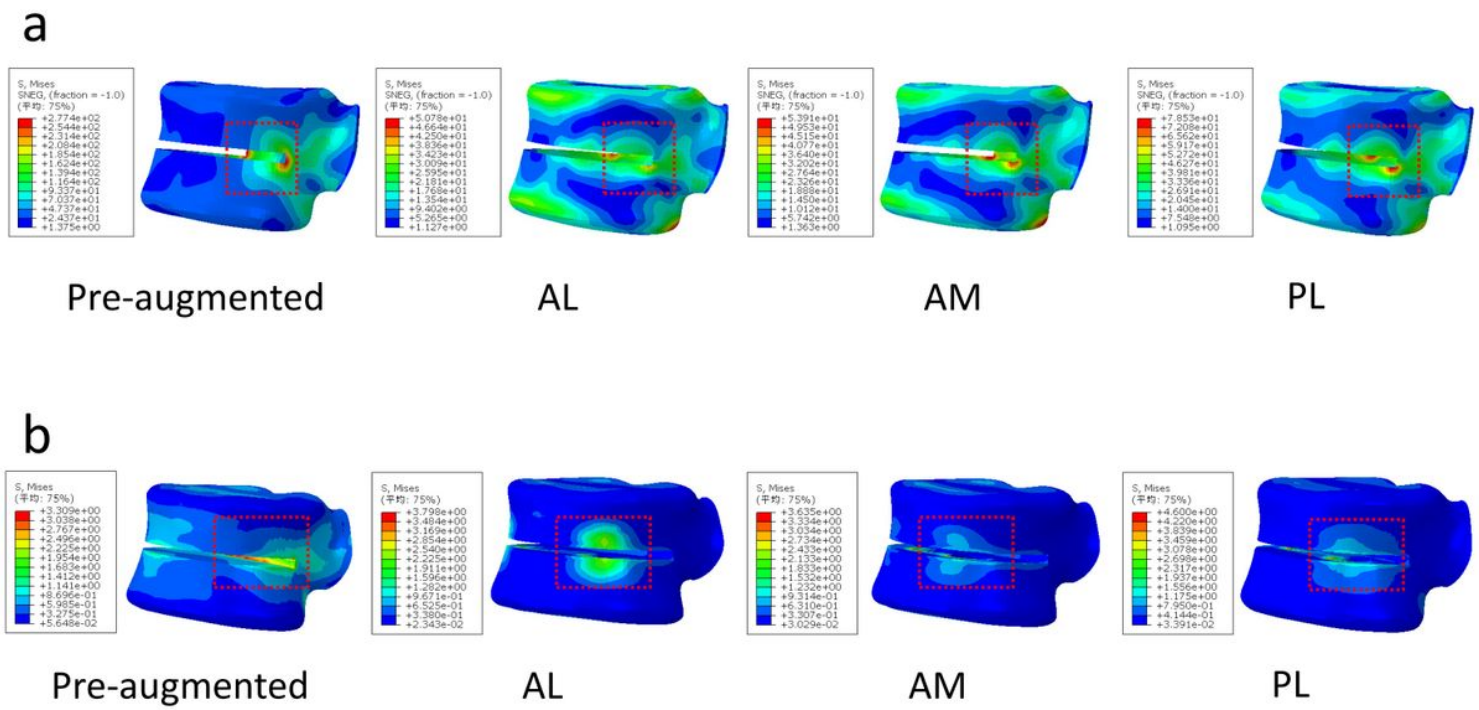

Figure 4

The nephograms of the von Mises stress under flexion in L3 for OVCF models before and after PVA. (a) Cotical bone. (b) Cancellous bone.

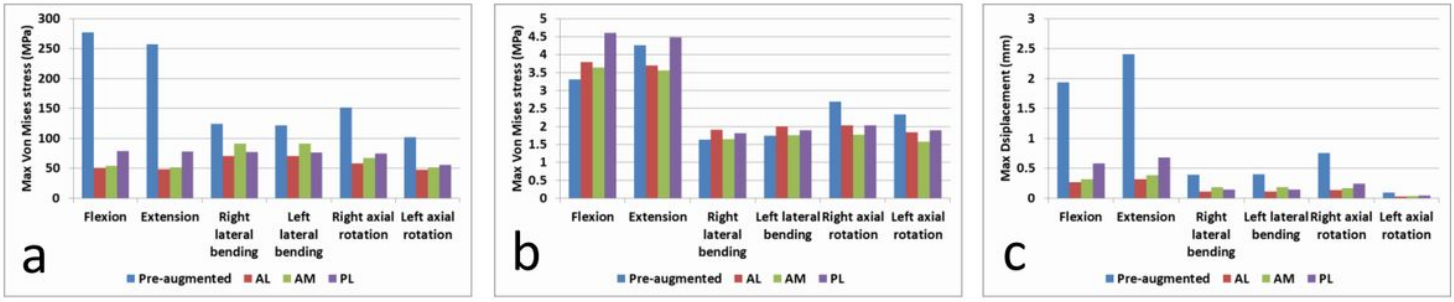

Figure 5

(a) The maximum von Mises stress in the cortical bone of L3. (b) The maximum von Mises stress in the cancellous bone of L3. (c) The maximum displacement of L3 vertebral body.